flowing liquid He cryostat. Thermal stability of the STM and the sample to within 0.01 K was reached 4 hours after initial cooling from room temperature.
13. Tips were made by etching polycrystalline tungsten wire in KOH. Tips were cleaned in UHV by repeated cycles of sputtering from field emission in a Ne atmosphere and annealing with an electron beam heater. Tips were sharpened just before the experiment by bringing the end of the tip in contact with the clean copper surface. Thus, the last atom on the tip is likely to be copper rather than tungsten. Cu(100) was cleaned with repeated cycles of 1 keV Ne^+ sputtering and annealing at 500°C until large defect-free regions of the surface were observed with the STM.
14. D. Arvanitis, U. Dobler, L. Wenzel, K. Baberschke, J. Stohr, *Surf. Sci.* **178**, 686 (1986).
15. X. F. Hu, C. J. Chen, J. C. Tang, *ibid.* **365**, 319 (1996).
16. Ts. S. Marinova and P. K. Stefanov, *ibid.* **191**, 66 (1987).
17. N. Sheppard, *J. Electron Spectrosc. Relat. Phenom.* **38**, 175 (1986).
18. Drifts were generally negligible during the time of each voltage sweep. With the feedback off, drift rates of ~0.001 Å min^{-1} and 0.01 Å min^{-1} were measured in the vertical and horizontal directions, respectively. By averaging spectra in the forward and backward sweep directions, the resulting small drift in the tunneling conductance was canceled out.
19. N. R. Avery, *J. Am. Chem. Soc.* **107**, 6711 (1985).
20. B. J. Bandy, M. A. Chesters, M. E. Pemble, G. S. McDougall, N. Sheppard, *Surf. Sci.* **139**, 87 (1984).
21. Supported by NSF grant DMR-9707195.

18 February 1998; accepted 15 April 1998

Combinatorial Electrochemistry: A Highly Parallel, Optical Screening Method for Discovery of Better Electrocatalysts

Erik Reddington, Anthony Sapienza, Bogdan Gurau, Rameshkrishnan Viswanathan, S. Sarangapani, Eugene S. Smotkin,* Thomas E. Mallouk*

Combinatorial screening of electrochemical catalysts by current-voltage methods can be unwieldy for large sample sizes. By converting the ions generated in an electrochemical half-cell reaction to a fluorescence signal, the most active compositions in a large electrode array have been identified. A fluorescent acid-base indicator was used to image high concentrations of hydrogen ions, which were generated in the electrooxidation of methanol. A 645-member electrode array containing five elements (platinum, ruthenium, osmium, iridium, and rhodium), 80 binary, 280 ternary, and 280 quaternary combinations was screened to identify the most active regions of phase space. Subsequent "zoom" screens pinpointed several very active compositions, some in ternary and quaternary regions that were bounded by rather inactive binaries. The best catalyst, platinum(44)/ruthenium(41)/osmium(10)/iridium(5) (numbers in parentheses are atomic percent), was significantly more active than platinum(50)/ruthenium(50) in a direct methanol fuel cell operating at 60°C, even though the latter catalyst had about twice the surface area of the former.

Combinatorial synthesis and analysis have become commonly used tools in bioorganic chemistry (*1*–*11*). Although the combinatorial (or multiple sample) approach to the discovery of inorganic materials has existed for more than two decades (*12*), new materials (*13*, *14*) and sensors (*15*) only recently have been discovered by this advanced Edisonian technique. There are several examples of combinatorial searches that have confirmed the properties of known materials (*16*, *17*) and catalysts (*18*). There are, however, no previous reports of superior catalysts that have been identified by combinatorial chemistry. Combinatorial searches for catalysts are often limited not by synthesis but by the lack of methods that can simultaneously screen many compositions. Recently, significant progress has been made in the thermographic screening of catalysts (*18*, *19*). We describe here a general combinatorial screening method for electrode materials and its application to the problem of anode catalysis in direct methanol fuel cells (DMFCs). By screening combinations of five elements (Pt, Ru, Os, Ir, and Rh), we found several good catalysts in unexpected regions of composition space and identified a quaternary catalyst with significantly higher activity than the best previously known catalyst (a binary Pt-Ru alloy).

Because methanol is a renewable liquid fuel, DMFCs present some distinct potential advantages over combustion engines and hydrogen fuel cells for transportation and remote power applications. They are silent and nonpolluting, and they use an easily distributed, high-energy-density fuel (*20*). One of the factors that limits their development and use is that known anode and cathode electrocatalysts produce useful current densities only at high overpotentials. The anode catalyst is particularly problematic, because it must perform a kinetically demanding reaction, the six-electron ($6e^-$) oxidation of methanol

$$CH_3OH + H_2O \rightarrow CO_2 + 6H^+ + 6e^- \quad (1)$$

Despite nearly three decades of research and optimization, the best known anode electrocatalysts are a binary Pt-Ru alloy (*21*) and a recently discovered Pt-Ru-Os ternary (*22*). The performance of these alloy catalysts is significantly enhanced relative to Pt alone. The bimetallic alloy is thought to work by a bifunctional or ligand effect mechanism, in which Ru activates water, and Pt activates the methanol C-H bond and also binds the CO intermediate in the reaction (*23*, *24*). Although binary alloys of Pt with many other oxophilic elements have been studied, none is more active than high-surface-area Pt-Ru. No predictive model for investigating ternary or quaternary combinations has emerged and, in fact, little is known about the phase equilibria of ternary and quaternary Pt alloys.

Although electrocatalysts are typically tested by measuring current as a function of potential, this approach becomes increasingly unwieldy as the number of samples increases. Successful uses of the combinatorial method—for example, massively parallel screening for biochemical affinity (*1*–*9*), organic host-guest interactions (*10*, *11*), and inorganic phosphorescence (*13*)—often use optical (absorption or emission) detection. Optical detection methods are fast regardless of the complexity of the array, are simple to implement, and allow one to ignore the uninteresting majority of phase space. This method can be adapted to electrochemical screening by recognizing that all half-cell reactions (for example, reaction 1) involve an imbalance of ions. Therefore, a fluorescent indicator that detects the presence or absence of ions (H^+ in the case of the DMFC anode) in the diffusion layer images the activity of the array.

This idea is illustrated in a small ternary Pt-Os-Rh array, prepared by manually pipetting appropriate metal salts and aqueous $NaBH_4$ onto Toray carbon paper (Fig. 1). The carbon substrate is electronically conducting but not catalytic for the oxidation of methanol. The array electrode serves as the working electrode in a single-compartment,

T. E. Mallouk, E. Reddington, A. Sapienza, Department of Chemistry, The Pennsylvania State University, University Park, PA 16802, USA.
E. S. Smotkin, B. Gurau, R. Viswanathan, Department of Chemical and Environmental Engineering, Illinois Institute of Technology, Chicago, IL 60616, USA.
S. Sarangapani, ICET, Inc., Norwood, MA 02062, USA.

*To whom correspondence should be addressed. E-mail: chemsmotkin@minna.acc.iit.edu (E.S.S.) or tom@chem.psu.edu (T.E.M.).

three-electrode cell and is stepped progressively into the potential region where methanol is oxidized. The electrolyte contains a fluorescent indicator, which is luminescent in its acid form but not in the base. Quinine and the Ni^{2+} complex of 3-pyridin-2-yl-<4,5,6>triazolo-<1,5-a>pyridine (PTP) (Scheme 1) (*25*) were used as indicators at

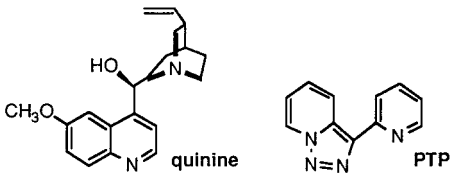

Scheme 1

neutral and low pH, respectively. At low overpotential, the quinine solution above the most active spot in the array fluoresces brightly and is surrounded by six neighboring compositions of lower activity. The Ni-PTP indicator fluoresces less brightly but is still adequate for identification of the most active areas by visual inspection. The best anode composition in this ternary array [Pt(62)/Rh(25)/Os(13); numbers in parentheses are atomic percent] is a much better catalyst than Pt and is slightly inferior to Pt(50)/Ru(50). Interestingly, this relatively active catalyst lies in a ternary region that is bounded by quite inactive binaries, Pt-Os and Pt-Rh; that is, it lies in a part of composition space where one would not expect to find good catalysts.

More compositionally diverse arrays must be intelligently designed because the number of compositions sharply increases with each added element. A simple way to map a quaternary phase diagram into two dimensions is to unfold it (Fig. 2). This mapping gives a smooth variation in composition across the array, as illustrated in the color map made from cyan, magenta, yellow, and black inks. At the resolution shown in Figure 2, a four-component array contains an outer shell of 4 elements (vertices), 48 binaries (edges), and 112 ternary (faces) compositions. There are two inner shells containing 52 and 4 quaternaries, for a total of 220 unique compositions. In practice, it is convenient to map all single, binary, ternary, and quaternary combinations of five elements into a rectangular pattern by eliminating the redundant binary and ternary spots. At the same resolution as the quaternary array shown in Figure 2, the resulting "five-pick-four" array (not shown) contains 645 different compositions, each with the same number of moles of metal per spot.

A common approach to generating large combinatorial arrays is by automation (*26*, *27*). By customizing a commercially available inkjet printer, we printed metal salt "inks" into quaternary and five-pick-four patterns. We adjusted aqueous inks prepared from $H_2PtCl_6 \cdot 6H_2O$, $RuCl_3 \cdot xH_2O$, $OsCl_3$, K_2IrCl_6, and $RhCl_3 \cdot 2.4H_2O$ to the appropriate viscosity by adding glycerol. A typical quaternary array, prepared by inkjet printing and subsequent borohydride reduction, is shown (Fig. 2) (*28*, *29*). After the arrays were dried, washed, and contacted electrically, they were screened for activity in methanol-indicator solutions (*30*). This procedure identified several active regions. Because the resolution of the large arrays was not sufficient to pinpoint the most active composition, active areas were magnified in "zoom" arrays printed from end-member ink mixtures that bounded each region. A typical zoom array had about three times the resolution of a large survey scan along any binary direction and therefore encompassed about 4% of the whole composition space.

Bulk samples of the most active compositions were characterized by powder x-ray diffraction, x-ray photoelectron spectroscopy, and rotating disk voltammetry, and were then tested as anode catalysts in DMFCs. A comparison of steady-state DMFC power curves obtained with the best quaternary catalyst deduced from the combinatorial analysis Pt(44)/Ru(41)/Os(10)/Ir(5) and the best commercially available Pt(50)/Ru(50) is shown (Fig. 3). The current density with the new quaternary catalyst is about 40% higher at 400 mV and more

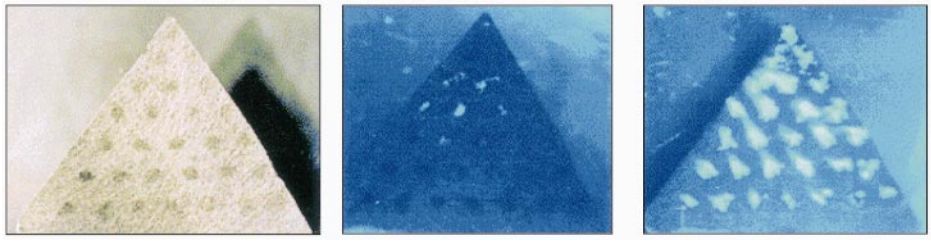

Fig. 1. Pt-Rh-Os ternary array in 6 M aqueous methanol (pH 6) quinine indicator. (**Left**) Image in white light. (**Center**) Fluorescence image at low overpotential, identifying the most active region of composition space. (**Right**) Fluorescence image at high overpotential, where methanol oxidation occurs at every spot in the array.

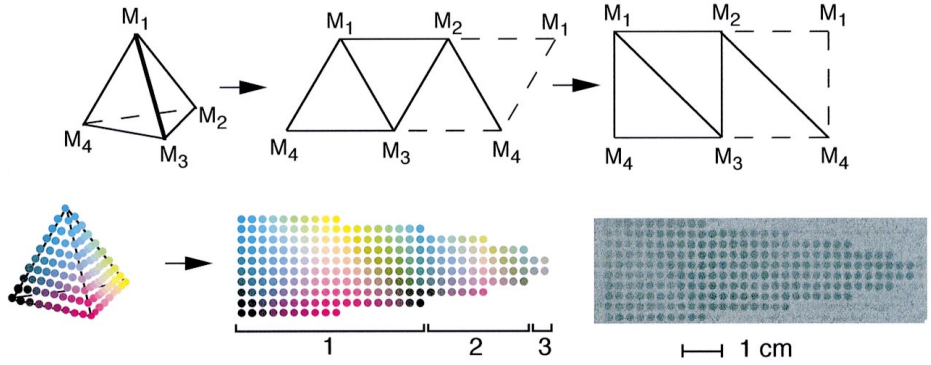

Fig. 2. (**Top**) Unfolding of a quaternary phase diagram and mapping into two dimensions. (**Lower left**) At a resolution of 10 different compositions along each binary edge, a quaternary map contains 220 unique spots, with composition varying smoothly across the array. Redundant binary lines (dashed lines in top drawing) are eliminated in the map. The three nested shells in the phase diagram are marked 1, 2, and 3 in the map. (**Lower right**) Borohydride-reduced, inkjet-printed array of electrocatalysts on Toray carbon paper.

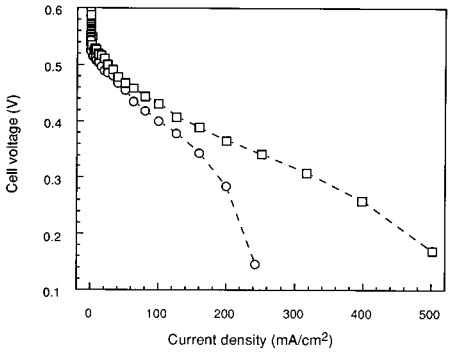

Fig. 3. Comparison of steady-state current-voltage data for direct methanol fuel cells made from Pt(44)/Ru(41)/Os(10)/Ir(5) (□) and Johnson–Matthey Pt(50)/Ru(50) (○) anode electrocatalysts. Anode: 4.0 mg/cm^2, 12.5 ml/min, 0.5 M methanol, 0 pounds per square inch gauge (psig); cathode: Pt at 4.0 mg/cm^2, 400 standard cubic centimeters per minute of dry air at 10 psig; cell: 60°C, Nafion 117 polymer electrolyte membrane. Cell potentials are compensated for series resistance.

than double that of Pt-Ru under short circuit conditions. This difference is especially striking when one considers that the Pt-Ru, prepared by a proprietary method, is an optimized, high-surface-area catalyst [measured Brunauer–Emmet–Teller (BET) surface area of 65 m^2/g]. The quaternary catalyst, made by borohydride reduction, is not optimized and has roughly half (31 m^2/g) the surface area. This difference indicates that the intrinsic activity of Pt-Ru-Os-Ir per surface atom is several times greater than that of Pt-Ru. Why the addition of relatively small amounts of Os and Ir causes such a substantial increase in activity is an interesting question, to which we currently have no answer.

This study illustrates some of the strengths of the combinatorial method as applied to catalysis. It is possible to search a fairly large phase space rapidly and exhaustively. Although the best catalyst is close in composition to previously known binaries and ternaries, it is markedly superior in performance. Although this catalyst might have been looked for by extrapolation of the binary and ternary results, a serial search of this composition space would be very time-consuming. Further, the combinatorial approach identifies active compositions in regions bounded by inactive binaries—that is, where a targeted, serial search would not normally be done. Finally, we note that the optical screening method developed for anode catalysts might be applied to various electrochemical materials problems (electrocatalysis, battery materials, corrosion) by using the appropriate fluorescent chemosensor molecules.

REFERENCES AND NOTES

1. S. P. Fodor *et al*., *Science* **251**, 767 (1991).
2. K. S. Lam *et al*., *Nature* **354**, 82 (1991).
3. R. A. Houghten *et al*., *ibid*., p. 84.
4. L. C. Bock, L. C. Griffin, J. A. Latham, E. H. Vermann, J. J. Toole, *ibid.* **355**, 564 (1992).
5. C. Y. Cho *et al*., *Science* **261**, 1303 (1993).
6. B. L. Bunin and J. A. Ellman, *J. Am. Chem. Soc.* **114**, 10997 (1992).
7. A. A. Virgilio and J. A. Ellman, *ibid.* **116**, 11580 (1994).
8. S. H. DeWitt *et al*., *Proc. Natl. Acad. Sci. U.S.A.* **90**, 6909 (1993).
9. D. A. Campbell, J. C. Bermak, T. S. Burkoth, D. V. Patel, *J. Am. Chem. Soc.* **117**, 5381 (1995).
10. M. H. Ohlmeyer *et al*., *Proc. Natl. Acad. Sci. U.S.A.* **90**, 10922 (1993).
11. M. Torneiro and W. C. Still, *J. Am. Chem. Soc.* **117**, 5887 (1995).
12. J. J. Hanak, *J. Math. Sci.* **5**, 964 (1970).
13. E. Danielson *et al*., *Science* **279**, 837 (1998).
14. R. B. van Dover, L. F. Schneemeyer, R. M. Fleming, *Nature* **392**, 162 (1998).
15. T. A. Dickinson, D. R. Walt, J. White, J. S. Kauer, *Anal. Chem.* **69**, 3413 (1997).
16. G. Briceño, H. Chang, X. Sun, P. G. Schultz, X.-D. Xiang, *Science* **270**, 273 (1995).
17. X.-D. Xiang *et al*., *ibid.* **268**, 1738 (1995).
18. F. C. Moates *et al*., *Ind. Eng. Chem. Res.* **35**, 4801 (1996).
19. S. J. Taylor and J. P. Morken, *Science* **280**, 267 (1998).
20. T. F. Fuller, *Electrochem. Soc. Interface* **1997**, 26 (1997).
21. M. Watanabe, M. Vehida, S. Motoo, *J. Electroanal. Chem.* **229**, 395 (1987).
22. K. L. Ley *et al*., *J. Electrochem. Soc.* **144**, 1543 (1997).
23. R. Parsons and T. Vandernoot, *J. Electroanal. Chem.* **257**, 9 (1988).
24. T. Frelink, W. Vissher, A. P. Cox, J. A. R. van Veen, *Electrochim. Acta* **40**, 1537 (1995).
25. H. Mori *et al*., *Chem. Pharm. Bull.* **41**, 1944 (1993).
26. A. V. Lemmo, J. T. Fisher, H. M. Geysen, D. J. Rose, *Anal. Chem.* **69**, 543 (1997).
27. A. P. Blanchard, R. J. Kaiser, L. E. Hood, *Biosens. Bioelectronics* **11**, 687 (1996).
28. D. W. McKee, *J. Catal.* **14**, 355 (1969).
29. Metal salts were printed with an Apple Color Stylewriter 2500 onto Toray carbon rectangles taped to ordinary paper. The pattern for each element was drawn in gray scale with commercial drawing software. The printer was calibrated by ultraviolet-visible spectroscopy by printing a highly absorbing organic dye onto transparencies and then desorbing each spot into a known volume of solution. The reduction step was carried out by clamping the array into a home-built Plexiglas device that provided solution wells in the quaternary or five-pick-four pattern. In each well, the printed metal salts were redissolved in a buffered solution (2 μl of 2 M $NaHCO_3$) and then reduced (1μl of 5% $NaBH_4$).
30. The aqueous indicator solution was 6 M methanol, 0.5 M $NaClO_4$, 30 mM $Ni(ClO_4)_2$, and 100 μM PTP adjusted to pH 3 with $HClO_4$. The carbon substrate has a small resistance (1 to 3 ohms), which translates to a negligible potential drop at the screening currents used (about 1 mA). Bulk samples of catalysts were prepared by dissolving the appropriate metal salts in water to attain an overall concentration of 2 mM. The pH was adjusted to 9, and a 10-fold excess of 5 weight % sodium borohydride was added at one drop per minute. The black precipitate was washed 10 times with water and dried at 110°C. Fuel cell membrane-electrode assemblies were constructed from Nafion 117 by preparing a suspension of the catalyst in 15 weight % soluble Nafion and painting the material onto a decal as described in detail in (*22*).

31. We thank A. Czarnik, D. L. Feldheim, R. Wodd, X.-D. Xiang, and P. G. Schultz for helpful discussions; Todd LaFrenz for performing BET measurements; and the Office of Naval Research (LBL Molecular Design Institute), the Defense Advanced Research Projects Agency, and the Army Research Office for financial support.

16 March 1998; accepted 6 May 1998

Compatibility of Rhenium in Garnet During Mantle Melting and Magma Genesis

Kevin Righter* and Erik H. Hauri

Measurements of the partitioning of rhenium (Re) between garnet and silicate liquid from 1.5 to 2.0 gigapascals and 1250° to 1350°C show that Re is compatible in garnet. Oceanic island basalts (OIBs) have lower Re contents than mid-ocean ridge basalt, because garnet-bearing residues of deeper OIB melting will retain Re. Deep-mantle garnetite or eclogite may harbor the missing Re identified in crust-mantle mass balance calculations. Oceanic crust recycled into the upper mantle at subduction zones will retain high Re/Os (osmium) ratios and become enriched in radiogenic ^{187}Os. Recycled eclogite in a mantle source should be easily traced using Re abundances and Os isotopes.

The Re-Os isotopic system provides constraints on the role of crustal recycling into Earth's deep interior (*1*). Both elements exhibit siderophile behavior in metal-silicate systems, yet in mantle and crustal melting environments, Re is thought to be strongly incompatible (partitioned into magma) and Os strongly compatible (partitioned into the residue) (*2*). Several aspects of the geochemical behavior of Re during mantle melting have remained uncertain. First, oceanic island basalts (OIBs) and some picrites have lower Re contents than mid-ocean ridge basalt (MORB) (*3*), but just the opposite is expected for an incompatible element controlled by the extent of partial melting. Second, the mass of Re in the primitive mantle cannot be balanced by the sum of the continental crust and depleted mantle reservoirs (*4*). Finally, oceanic crust with a high Re/Os ratio is injected into the mantle at subduction zones, yet it is not known whether the Re is lost to fluids in the subduction zones or is retained in eclogite and recycled back into the mantle.

Rhenium is incompatible in most silicate phases such as clinopyroxene and olivine (*5*), but its behavior in garnet-bearing systems at depths >100 km in the mantle has been uncertain. Several observations suggest that garnet may play a role in fractionating Re from Os. Garnet separates from a garnet pyroxenite have almost 10 times more Re than the bulk rock (*6*). Data from oceanic basalts show that Re and Yb behave similarly during mantle melting (*3*); and because Yb is compatible in garnet (*7*), a similar behavior has been hypothesized for Re (*3*). Re-Al_2O_3 systematics in orogenic lherzolites also suggest a link between Re and garnet (*8*). In order to better under-

K. Righter, Lunar and Planetary Laboratory, University of Arizona, Tucson, AZ 85721, USA.
E. H. Hauri, Department of Terrestrial Magnetism, Carnegie Institution of Washington, Washington, DC 20015, USA.

*To whom correspondence should be addressed. E-mail: righter@lpl.arizona.edu